HHS Public Access

Author manuscript

IEEE J Sel Top Quantum Electron. Author manuscript; available in PMC 2017 January 02.

Published in final edited form as:

IEEE J Sel Top Quantum Electron. 2012 ; 18(4): 1465–1477. doi:10.1109/JSTQE.2012.2185823.

Fluorescence Lifetime Spectroscopy and Imaging in Neurosurgery

Laura Marcu and **Brad A. Hartl**

University of California, Davis, Davis, CA 95616 USA

Abstract

Clinical outcome of patients diagnosed with primary brain tumor has been correlated with the extent of surgical resection. In treating this disease, the neurosurgeon must balance between an aggressive, radical resection and minimizing the loss of healthy, functionally significant brain tissue. Numerous intra-operative methodologies and technological approaches have been explored as a means to improve the accuracy of surgical resection. This paper presents an overview of current conventional techniques and new emerging technologies with potential to impact the area of image-guided surgery of brain tumors. Emphasis is placed on techniques based on endogenous fluorescence lifetime contrast and their potential for intraoperative diagnosis of brain tumors.

Index Terms

Autofluorescence; brain tumor; fluorescence; glioma; imaging; neurosurgery; spectroscopy; surgery

I. Introduction

BRAIN and central nervous system (CNS) tumors are expected to account for 13 110 deaths and 22 340 new cases in the United States in 2011 according to the National Cancer Institute [1]. This provides the basis for an estimated $3.7 billion that is spent on brain cancer treatments annually [2]. Furthermore, these types of tumors are the leading cause of death from solid tumor cancer in children [2]. Gliomas and meningiomas are the two most common types of brain and CNS tumors, accounting for 36% and 32% of all cases, respectively [3]. Glioblastoma multiforme (GBM), the most aggressive and common glial tumor, has a five-year mean survival rate of only 4% [1]. Gliomas arise due to an accumulation of genetic and chromosomal alterations in non-neuronal glial cells, which provide a variety of support functions for the neurons in the CNS. Gliomas are generally classified in two ways, by their cell type and tumor grade. Cell types can consist of either ependymoma, astrocytoma, oligodendroglioma, or a combination of these. A grading system is then used to further classify the tumor based on pathologic evaluation. The World Health Organization classification system is the most common, and consists of grades I through IV. Low-grade gliomas (LGG)—grade I and grade II—are nonmalignant and can often be treated with surgical resection alone or in combination with radio- and chemotherapy [4].

Color versions of one or more of the figures in this paper are available online at http://ieeexplore.ieee.org.

High-grade gliomas (HGG)—grade III and grade IV—are considered malignant and are histologically highly heterogeneous, containing both stromal and neoplastic tissues [5]. Grade IV tumors, including GBM, are mitotically active, necrosis-prone neoplasms and are usually associated with swift disease progression and a fatal outcome.

A. Current Treatment Practices

Current treatment for malignant brain tumors typically consists of surgical resection followed by chemoradiotherapy [6]. It has been shown that the extent of surgical resection is the single most important factor for long-term survival [7], [8]. Extent of resection is conventionally determined by calculating the volume of enhanced signal intensity in both pre- and postoperative T1-weighted contrast-enhanced images (T2-weighted for nonenhancing tumors) [9]. Due to the tumor's infiltration into the normal brain parenchyma, complete resection is difficult to achieve without removing healthy, functionally significant tissue [6]. Therefore, surgeons must balance between an aggressive, radical resection and minimizing the loss of healthy, functionally significant brain tissue. Commonly used tools to aid the surgeon in resection include image-guided stereotaxy, intraoperative ultrasound, and biopsies. Although intraoperative biopsies can provide definite pathological identification, this can take on the order of 20 min and is only used on a limited basis. Table I summarizes the advantages and limitations of techniques used in standard care in neurosurgery as well as emerging new techniques and methodologies tested in the clinical setting. An ideal technique for glioma resection would provide feedback to the surgeon in real time, have resolution at least as great as clinical MRI systems, and be able to detect tumor tissue below the exposed surface.

1) Stereotactic Image-Guided Surgery With Preoperative Imaging Scans— Stereotactic image-guided surgery uses preoperative images coregistered with either an optical or electromagnetic tracking system, allowing the surgeon to identify the location of tools with respect to a high contrast image. One of the largest limitations of stereotactic image-guided surgery is the loss of registration due to the brain's shift and deformation during surgery. This can be caused by tumor removal, brain swelling, or cerebrospinal-fluid drainage and can result in positioning errors on the order of 1 cm. Further error is introduced by the tracking system, which typically falls in the range of 2–5 mm [10]. Although frame-based systems can provide improved accuracy up to 1 mm or less, they are infrequently used due to the ease of use and simplicity of their frameless-based competitors.

2) Intraoperative Ultrasound—Intraoperative ultrasound is not limited by brain shift and represents a simple tool that provides subsurface structural imaging, albeit at lower resolution and limited penetration. Intraoperative systems typically use end-fire transducers that operate in the 5–15 MHz region and have the capability to perform color Doppler sonography for vascular delineation [38], [39]. Penetration depth is dependent upon the frequency used and can range from 3 to 10 cm. Correspondingly, axial and lateral resolution can range from 0.15 to 0.35 mm and 0.4 to 1.2 mm, respectively [12]. Studies have shown that it can be a quick and reliable method to determine a tumor's location and evaluate the completeness of resection [14], [40]. However, a steep learning curve involving an extensive

amount of practical use and poor signal-to-noise ratio (SNR) have prevented a more widespread use of it by surgeons [38].

3) Intraoperative Magnetic Resonance Imaging—In order to overcome the issues of brain shift and the limited resolution of ultrasound, intraoperative magnetic resonance imaging (iMRI) has been studied as a tool to aid in tumor resection [10], [41]–[43]. Both high (1.5–3 T) and low (0.12–0.5 T) field iMRI setups have been studied in the clinical setting. High-field units have the advantage of being able to provide higher resolution and shorter scan times, but suffer from the need to either use nonferromagnetic surgical tools or place the magnet in an area adjacent to the surgical suite [44]. In either case, considerable measures are usually taken to reduce the radiofrequency noise generated by the variety of electronics found in an operating room. Low-field iMRI units use weaker magnets that limit achievable resolution, but also eliminate the need to move the patient for scans or use nonferromagnetic surgical tools [45]. Although some iMRI systems can produce similar resolution to preoperative systems, due to the disruption of the blood–brain barrier (BBB) during surgery, Gadolinium is ineffective as a contrast agent [46]. Therefore, intraoperative images often do not provide the same contrast as those taken preoperatively. iMRI's efficacy is also limited by how frequently scans are made during the procedure. Scans typically take a few minutes but can accumulate to increase the surgery time by roughly 1 h [19]. In addition to significant maintenance costs that will exist for the extent of its lifetime, installation costs for these units can be on the order of $3–8 million [19]. Studies have shown that a more complete extent of resection can be achieved with iMRI [47], [48], but further clinical trials are required in order to make conclusions regarding patient survival and quality of life [18], [19]. Ultimately, iMRI systems are mostly found in academic medical centers due to their inherent limitations and the large overhead costs.

B. New Techniques in Clinical Studies

1) Exogenous Contrast Agent—A considerable amount of clinical studies have been performed using exogenous contrast agents to aid in fluorescence-guided resection (FGR) of brain tumors. Contrast agents are typically injected intravenously and tend to localize to the tumor due to the breakdown of the BBB and the enhanced permeability and retention effect [49]. Fluorophore excitation can be achieved by a variety of methods including filtered and unfiltered white light and lasers. The first clinical use of FGR employed fluorescein sodium and was studied by Moore *et al.* [50]. Fluorescein sodium saw little use since then but considerable interest has been renewed in the last decade [51]–[55]. Despite its inability to distinguish between different grades of lesions [54], fluorescein sodium can allow for safe and simple FGR.

Attempts have been made to employ indocyanine green (ICG) using an enhanced optical imaging setup for FGR [56] and also more recently using microscope-integrated videoangiography [57], [58]. Presently, ICG has not been implemented to successfully demarcate tumor margins. This is likely due to its binding to albumin in blood [59], which prevents it from crossing intact BBB and cell membranes [60].

Meta-tetrahydroxyphenylchlorin (mTHPC, Tempoforin, Foscan) has also been employed in FGR [61] and FGR combined with PDT [23], [62], [63]. Similar to the previous two contrast agents, mTHPC extravasation is observed with disruption of the BBB [64], although it does appear to localize favorably in tumor tissues [65]. When used for standalone FGR, the fluorescence of GBM tumors was correlated with the histological analysis with 88% sensitivity and 96% specificity [61]. However, in addition to increased intracranial pressure [66] and damage to healthy tissue [67], [68], light hypersensitization of skin lasting four weeks after the procedure was also observed in patients receiving injections of mTHPC [23].

2) Biochemical Imaging Agents—The most well-studied FGR system is the use of the prodrug 5-aminolevulinic acid (ALA, Gliolan) to induce hyperactivity in the heme production pathway. This provides fluorescently detectable levels of protoporphyrin IX [69]–[71], of which higher levels are found in tumor tissues [72]–[75]. To date, the largest clinical effort has been performed by Stummer *et al.* [74]. Initial studies performed by this group on ten patients detected malignant tissue against tissue biopsies with 85% sensitivity and 100% specificity [76]. Subsequently, their randomized phase-III trial showed that ALA mediated FGR resulted in significantly more complete resections (65% versus 35%), which increased the mean survival time by 4.9 months with respect to patients not receiving FGR [77]. A significant amount of clinical studies have also been performed in Japan [78]–[83] and Switzerland [84], and by the Dartmouth group [84], [85]. Clinically, ALA has also been implemented in spectroscopy studies [86]–[89], endoscopy-type imaging systems [78], and also in combined FGR-PDT [63]. Studies thus far have reported ALA to be useful for the detection of high, but not low-grade tumors [90], and have shown promise for the detection of meningiomas [81], [83]. Studies have also highlighted its lack of specificity, noting that it localizes to any abnormal tissue, including tumorous, necrotic, or demyelinating types [78], [79], [82]. Skin photosensitivity for ALA is a notable improvement over mTHPC, and lasts only a few hours after injection [22].

3) Endogenous Fluorescence—In an attempt to circumvent the need for an injectable contrast agent, several studies have utilized naturally occurring fluorophores to identify tumor boundary information. These include nicotinamide adenine dinucleotide (phosphate) (NAD(P)H), flavin adenine dinucleotide, collagen, porphyrins, glutamate decarboxylase (GAD), and pyridoxamine-5-phosphate (PMP) and its derivatives. NAD(P)H is one of the most studied fluorophores in brain tissue. The reduced forms of NAD(P)H emit in the 400–490 nm spectral region while the oxidized forms ($NAD(P)^+$) are nonfluorescent [27], [91]. Among cancerous and noncancerous tissue types, variations in autofluorescence emission intensities have been attributed to differences in their NAD(P)H concentrations and to differences in their cellular redox states [91], [92]. Many highly proliferative cancers, including GBM, have enhanced nonoxidative glycolysis in a setting of either impaired or enhanced oxidative metabolism.

Differences in the decay spectra of the autofluorescent intensities between cancerous and normal tissues have been attributed to the disparities between the free and protein-bound forms of NAD(P)H [93]. Several commonly found genetic mutations in GBM (notably TP53, c-Myc, and IDH1) encode for proteins that can increase mitochondrial content or alter

the activities of cellular and mitochondrial dehydrogenases utilizing nicotinamide adenine dinucleotides [5], [94]. The metabolic consequences of these oncogenic mutations have been proposed as providing important cellular contributions that alter the protein-bound content of NAD(P)H.

Initial clinical studies were performed by Bottiroli *et al.* [92] using a fiberoptically coupled filtered mercury lamp excitation source and spectrograph in a point spectroscopy setup. In a subsequent study, healthy white and gray matter and neoplastic lesions were measured in a total of 12 patients during resection procedures [91]. Their system employed a mercury lamp as an excitation source (366 nm) and a bundle of 20 optical fibers—4 excitation (200 μm diameter) and 16 collection (50 μm diameter)—as a conduit for the delivery and collection of light. For the acquisition of spectra, room lights in the operating room were turned OFF. Classification of the data was not attempted.

In addition to point-spectroscopy autofluorescence spectral information, the Mahadevan–Jansen group has combined these measurements with white light diffuse reflectance spectroscopy in the clinical setting [25]–[28]. Their setup utilizes a nitrogen laser (337 nm) for fluorescence excitation and a bundle of seven optical fibers with 300 μm core diameters to facilitate the delivery (two fibers) and collection (five fibers) of photons Fluorescence and diffuse reflectance spectra were recorded from 350 to 800 nm and 400 to 800 nm, respectively. In initial studies, tumor margins were discriminated from normal brain tissue in 26 patients with sensitivity and specificity of 100% and 76%, respectively [25]. In a similar follow-up study of 24 patients, they reported 94% sensitivity and 93% specificity for discerning tumor margin from healthy tissue and 80% sensitivity and 89% specificity for solid tumor differentiation from healthy tissue [26]. For these studies, data were processed postoperatively and utilized empirical discrimination algorithms to analyze background, fluorescence, and diffuse reflectance spectra in order to predict tissue type against histopathological results from biopsies. Studies were also performed using diffuse reflectance and fluorescence spectral imaging techniques; however, measurements were made on only one patient [28]. Ultimately, these types of intensity measurements still suffer from variability stemming from blood absorption on the surface of the sample. This presents a notable issue as blood is often present at the interface between the resection margin and the infiltrating tumor.

More recently [95]–[98], fluorescence lifetime contrast has been studied as a means of improving the specificity of fluorescence measurement by capitalizing on the additional dimension of fluorescence emission, namely the excited state lifetime(s). By applying spectrally resolved lifetime measurements, higher information content can be obtained from a point measurement when compared to emission spectrum measurement alone. Time-resolved fluorescence measurements provide a means of resolving biological fluorophores with overlapping emission spectra but with different fluorescence decay times. The measurements can also yield more robust quantitative measurements *in vivo* since they are independent of intensity. This paper reviews the time-resolved fluorescence studies conducted in human primary brain tumors both in *ex vivo* specimens [30], [31], [35] and intraoperatively in patients [32], [33] undergoing brain tumor surgery.

II. Fluorescence Lifetime Techniques

A. Instrumentation

Several developments of fluorescence lifetime instrumentation for tissue diagnosis have been reported over the past two decades [95], [97], [99], [100]. This includes spectroscopy systems for point measurements (single channel) [29], [36], [101]–[103] and imaging spectroscopy (multiple channels) [34], [104], [105] devices. The multichannel implementation also known as fluorescence lifetime imaging microscopy (FLIM) includes both wide-field [34], [97], [106] and scanning [36] systems. FLIM allows the localization and mapping of fluorophore distributions so that structural, chemical, and environmental information may be contrasted across the field of interest. The majority of these instruments, however, were primarily used for *ex vivo* characterization of tissue specimens. Only a small number of devices based on fluorescence lifetime were used in clinical environments. To our knowledge, only two such instrumental setups were used for intraoperative measurements of brain tumors [29], [32]–[34]. These are briefly reviewed in the following.

1) Time-Resolved Fluorescence Spectroscopy—The time-resolved fluorescence spectroscopy (TRFS) apparatus (see Fig. 1) used for the investigation of brain tumors was based on a pulse sampling technique that allows for fast recording of spectrally resolved fluorescence decays, thus reconstruction of the emission spectrum along with the wavelength-dependent decay characteristics. A full description of this instrument was reported previously [29], [32], [33]. Main components include a pulsed nitrogen laser (MNL200, Lasertechnik, Berlin) as an excitation source (337 nm, 700 ns pulse width, and 50 Hz maximum repetition rate); a sterilizable fiber-optic probe for light delivery and collection as described later; an *f*/4 dual mode imaging spectrograph (250 is/sm, Chromex, Inc.) for fluorescence light dispersion; a fast gated multichannel plate photomultiplier tube (MCP-PMT: rise time of 180 ps, bandwidth up to 2.0 GHz, R5916-50, Hamamatsu) for fluorescence detection; a digital oscilloscope (1 GHz, 5 Gsamples/s sampling rate, TDS5104, Tektronix) for fluorescence response pulse sampling; a computer workstation for automated instrument control and data acquisition; and peripheral electronics. The bifurcated fiber optic probe (nonsolarizing silica/silica step index fibers of numerical aperture (NA) 0.11; central excitation fiber of 600 μm surrounded by a ring of 12 200 μm collection fibers) was custom made. To improve the collection efficiency of this probe, the collection fibers were polished at a bevel angle of 10°. For this bifurcated probe, the maximum collection efficiency was at about 3 mm above the tissue surface. It was found that the minimum SNR required for an adequate estimation of the TRFS parameters was ~40. For the experiments conducted in humans, the excitation energy (at the tip of the fiber probe) was 3.0 μJ/pulse. The area illuminated by the probe was 2.654 mm^2; thus, the total fluence per pulse received by the tissue was 1.39 $\mu J/mm^2$, a value within the approved ANSI standard limits for UV exposure. This instrument has temporal resolution of less than 300 ps and can provide nanomolar sensitivity. Recording of the entire spectrally and temporally resolved emission spectrum (360–550 nm) takes less than 30 s and can be performed under normal room light.

2) Fluorescence Lifetime Imaging Microscopy (FLIM)—The fluorescence lifetime imaging microscopy (FLIM) apparatus (see Fig. 2) adapted to the clinical setting was based on a wide-field imaging technique that uses a fast-gated intensified CCD (ICCD) camera as a detector. This system was described in earlier publications [34], [104], [105]. Tissue fluorescence was induced by the same pulsed (700 ps pulse width) nitrogen laser used in TRFS measurements described earlier and coupled to a separate high NA (0.4) 200 μm core diameter polymer fiber. The fluorescence emission was collected using a gradient index objective lens (NA of 0.5, 0.5 mm diameter, 4 mm FOV) cemented to a fiber image guide (0.6 mm diameter, 2 m long, 10 000 fibers). A 20× microscope objective and a 150-mm focal length achromatic lens were used to magnify fluorescence images onto the ICCD. The system allows for selection of up to six wavelength bands of interest via a motorized filter wheel. Two filters (center wavelength/bandwidth) 390/70 and 450/65 nm were used in the experiments. The incorporation of advanced electro-optics and fiber optics enabled the compact and robust design of this FLIM apparatus. A key component of this instrument was a compact ICCD (4 Picos, Stanford Computer Optics) camera with fully integrated electronic and optical devices in a small enclosure 24×14×11 cm^3, including a multichannel plate (MCP) image intensifier, relay lenses, a CCD camera, a delay generator, and a high-voltage power supply. The gate width was 0.2 ns for a repetition rate up to 200 kHz and the temporal resolution of the system was <0.5 ns. The energy density delivered at the tissue surface was 0.16 mJ/cm^2 per pulse.

3) Data Analysis—The fluorescence intensity decay profiles resulting from time-resolved measurements of tissues are often complex. Typically, several fluorescent molecular species in tissues are excited simultaneously. Consequently, the measured fluorescence decay represents the superposition of all individual decay components and cannot be fit by a single-exponential decay model. Moreover, the shape of the measured fluorescent pulse transient is affected by the opto-electronic components of the instrumental apparatus or instrument response.

Mathematically, the measured fluorescence intensity decay data $y(n)$ are given by the convolution of the fluorescence impulse response function (FIRF) $h(n)$ with the instrument response $x(n)$ [95], [97], [107]. In the discrete-time case, the relationship between the observed fluorescence intensity decay pulse and the excitation laser pulse is expressed by the convolution equation

$$y(n) = T \cdot \sum_{m=0}^{K-1} h(m)\, x(n-m), \quad n = 0, \ldots, K-1$$

where the parameter K determines the length of the fluorescence decay (IRF) or the extent of system memory, n is the number of time samples recorded for both $y(n)$ and $x(n)$, and T is the sampling interval (time resolution of the instrument). Computational methods for the evaluation of FIRF from tissue fluorescence measurements encompass a way to best estimate the shape of florescence decay and a rapid method for deconvolution.

Traditionally, the FIRF is approximated by a multiexponential decay and the most commonly used deconvolution method is least-squares iterative reconvolution (LSIR) [108], [109]. LSIR applies nonlinear least-squares optimization methods (e.g., Gauss–Newton and Lavenberg–Marquardt) to estimate the parameters of a multiexponential FIRF that would best fit its convolution with the system response to the fluorescence decay data

$$h(n) = \sum_{i=1}^{M} A_i e^{(-n/\tau_i)}.$$

Since the optimization process involves iterative convolutions, LSIR is computationally expensive. An alternative model-free deconvolution method for application to fluorescence decay data analysis uses expansion of the FIRF on a set of Laguerre basis functions [107], [110]. This approach was found to provide significant advantages over the more traditional methods when applied to tissue characterization. This method was used by our group for the analysis of brain tissues fluorescence decay characteristics and is based on the expansion of the kernels on an orthonormal set of discrete-time Laguerre functions (LF) $b_j^{\alpha}(n)$:

$$h(n) = \sum_{j=0}^{L-1} c_j^{\alpha} b_j^{\alpha}(n)$$

where c_j^{α} are the unknown Laguerre expansion coefficients, which are to be estimated from the input–output data, $b_j^{\alpha}(n)$ denotes the *j*th-order orthonormal discrete LF, and *L* is the number of discrete LF used to model the FIRF, e.g., order of the expansion. The LF basis is defined as $b_j^{\alpha}(n) = \alpha^{(n-j)/2}(1-\alpha)^{1/2}\sum_{k=0}^{j}(-1)^k \binom{n}{k}\binom{j}{k}\alpha^{j-k}(1-\alpha)^k, n \geq 0$. The functions of higher order converge slower to zero. The Laguerre parameter α ($0 < \alpha < 1$) determines the rate of exponential (asymptotic) decline of the discrete LF. Commonly, the parameter α is selected based on the kernel memory length *K* and the number of LF *L* used for the expansion, such that all the functions decline sufficiently close to zero by the end of the impulse response [107]. This method was found to provide important advantages over the more traditional methods when used in the context of tissue characterization [32], [33], [111], [112]. A brief summary of such advantages are given next.

First, no *a priori* assumption of the FIRF functional form of the decay dynamics is required. For complex biological systems, this feature is important as *a priori* imposition of the number of exponential components (conventional approach) may not readily provide a true representation of the underlying fluorescence dynamics. Second, the Laguerre expansion includes a built-in exponential term; thus, the LF are suitable for physical systems with asymptotically exponential relaxation dynamics [107], [110]. Third, since the Laguerre basis is a complete orthonormal set of functions, it can always provide a unique and complete expansion of the fluorescence dynamics (decay function). Fourth, it enables a fast deconvolution of input from the output, as it resumes to solving a linear least-squares minimization problem. For example, 35 fluorescence decay transients can be deconvolved in less than 1 s, or 480×736 pixel FLIM images in less than 60 s (2.40 GHz Intel Core 2 CPU

6600 and 1-GB RAM running Matlab) [34]. Fifth, the Laguerre coefficients can serve as additional parameters for fluorescence system characterization.

III. Time-Resolved Fluorescence of Brain Tumor Measured *Ex Vivo*

A. Glioma Studies

An initial TRFS study of brain tumors reported in 2004 [30] was conducted in specimens diagnosed as GBM Grade IV obtained during craniotomy. This study included 23 point measurements [9] from GBM, [9] from normal cortex (NC), and [5] from normal white matter (NWM)] and was the first to demonstrate the time-resolved fluorescence characteristics of brain tissue. The radiative lifetime of brain tumor tissue was found longer when compared with NWM and NC across all emission wavelengths (360–520 nm). The average lifetime values (~1.3 ns in tumor) at 460 nm emission suggest that the GBM fluorescence is likely dominated by the bound form of NAD(P)H fluorescence, whereas the relatively shorter lifetime (~1 ns) fluorescence of normal tissue is generated by a larger contribution of free-form NAD(P)H. In addition, this study showed that upon 337 nm excitation both tumor and normal tissue exhibit a second-peak fluorescence centered at about 390 nm. However, this peak was most prominent in GBM.

A subsequent study reported in 2006 [31] presents a more extensive (45 sites: 10 LGG, 15 HGG, 6 HGG with necrotic changes (HGGN), 5 NC, and 9 NWM) evaluation of TRFS's ability to distinguish between distinct types of brain tumor tissues including LGG, HGG, and HGGN from NC and NWM. Similar to the earlier study, two wavelength ranges were found important in distinguishing gliomas from normal brain tissue: 370–400 nm (the region of main peak emission for HGGN and NWM) and 440–480 nm (the region of main peak emission for NC as well as LGG and HGG). Interestingly, the LGG (~1.1 ns average lifetime at 460 nm) exhibited faster decay dynamics than HGG (~1.3 ns) with 95% confidence using Welch's *t*-test. The fluorescence characteristics of LGG measured *ex vivo* were found similar to those of NC but very different from that of NWM that presented a much slower decay dynamics (~1.8 ns at 460 nm). These characteristics were also corroborated with the NAD(P)H emission. The fluorescence emission characteristics of HGGN were found very distinctive from all other tissue types in both spectrum- and time-domain. The emission of this tumor type was dominated by a strong peak centered at about 380–390 nm with an average lifetime of ~2 ns, characteristics associated with the emission of connective tissue proteins. In particular, collagen formed in response to previous radiation treatment is likely to dominate the fluorescence emission of these tumors. Stepwise linear discriminant analysis applied to the TRFS-derived parameters had shown that different grades of gliomas, NWM, and NC tissues can be differentiated against histology using a relatively limited number of predictor variables (5 in total) from the two spectral ranges noted earlier. Parameters obtained from both spectral- (intensity values) and time-resolved emissions contributed to the accuracy of tissue classification. Resulting discriminate functions were used with the "leave one out" method to generate the test/training set for classification. Although a small database was used in this study, the reported results indicate that the time-resolved fluorescence spectroscopy technique is robust enough to allow good discrimination of LLG from NWM (sensitivity 90% and specificity 100%) as well a very

good delineation of brain tissue exposed to radiation therapy (sensitivity 83% and specificity 100%).

B. Meningiomas

TRFS was also investigated as an adjunctive tool for the intra-operative rapid evaluation and delineation of meningiomas [35]. Surgical resection is the main treatment for meningiomas causing symptoms and the extent of tumor resection directly correlates with prevention of recurrence. In this study, experiments were conducted in specimens from 26 patients (97 sites). The TRFS characteristics of meningioma were contrasted against those of the surrounding normal dura tissue as well as the cerebral cortex. As noted [35], certain intracranial characteristics of meningiomas can increase the difficulty of achieving a complete surgical resection. The *en plaque* variety and petroclival location of meningiomas are examples that often present complexity in excising dura involved with the tumor. Also, some meningiomas can invade the subjacent brain parenchyma, typically the cerebral cortex.

The fluorescence emission characteristics of meningiomas were found distinctive from that of both normal dura and cerebral cortex. Parameters derived from both spectral- and time-domain enabled discrimination of meningioma tissue. Overall, both meningioma and dura presented a distinct peak emission at about 390 nm, suggesting the strong contribution of collagens fluorescence. Collagen types I, III, and IV, as well as procollagens, laminins, and vimentin, are known constituents of meningiomas [113]–[115], whereas pyridinoline collagen cross links and an age-related fluorescence due to acceleration of collagen browning were reported as fluorophores within the dura [116]. At the 390 nm peak emission, the average fluorescence lifetime of normal dura (~1.7 ns) was found shorter than that of meningioma tissue (~2.0 ns). A reverse trend was reported for 460 nm emission associated with NAD(P)H fluorescence where dura (1.4 ns) presented a lifetime longer than that of meningioma (1.2 ns). The use of parameters derived from time-resolved measurements in a discriminant analysis scheme showed discrimination of meningioma with 89% sensitivity and 100% specificity. This study was the first to establish the feasibility of using TRFS as a tool for the identification of meningiomas and supports further development of real-time diagnostic tools for analyzing surgical tissue specimens of meningioma.

IV. Time-Resolved Fluorescence of Brain Tumor Measured *In Vivo* in Patients

A. Time-Resolved Fluorescence Spectroscopy of Glioma

The intraoperative application of TRFS was demonstrated in two studies [32], [33] of 17 and 42 patients, respectively; both were conducted in patients undergoing surgical removal of brain tumors. The fluorescence emission of several types of tumors was investigated including LGG (oligodendroglioma, oligodendrocytoma, and diffuse astrocytoma), intermediate grade (anaplastic astrocytoma), and HGG (anaplastic oligodendroglioma, anaplastic oligoastrocytoma, and GBM). The intra-operative measurements were conducted with the TRFS apparatus described earlier. Areas identified as glial tumors based on preoperative MRI (see Fig. 3) and surgeon experience were TRFS interrogated during surgical resection. Fig. 3(c) and (d) depicts examples of TRFS datasets (spectrally resolved

fluorescence decay profiles) for one-point measurement. Such datasets were acquired in less than 30 s. By using the Laguerre deconvolution method presented earlier, the recovery of this complete set of decay profiles took less than 2 s. In the first study during TRFS investigation, the fiber-optic probe was positioned above the areas of interest using a Greenburg retractor in order to minimize the probe positioning artifacts. In the second study, a spacer with two slits [see Fig. 1(c)] on opposite sides was added in front of the distal end of the probe. This latter configuration allowed the probe to be in contact with the tissue while maintaining a fixed distance from the tissue. The slits on the spacer also enabled suction of fluids to maintain a clear field.

These reports showed that the fluorescence emission of LGG has distinctive fluorescence emission characteristics enabling their discrimination from NC and NWM. For example, LGG (oligoastrocytoma and oligodendroglioma) measured *in vivo* [32] displayed a main peak emission at about 460 nm (see Fig. 4) that indicates NAD(P)H as the main biological fluorophore contributing to LGG fluorescence emission in contrast with normal tissues that presented a secondary peak at about 390 nm. Moreover, LGG presented faster fluorescence decay dynamics (~1 ns at 390 nm and ~0.6 ns at 460 nm) relative to NC and NWM (~2 ns at 390 nm and ~1 ns at 460 nm). Interestingly, a more extensive analysis of LGG based on tumor genetic subclassification reported subsequently [33], including diffuse astrocytomas, showed that this LGG tumor type presents longer lasting decay dynamics (e.g., ~1.5 ns at 390 nm) when compared to oligoastrocytoma and oligodendroglioma. These results have indicated that the LGG fluorescence emission varies with tumor phenotype or genetic subclassification. This finding [33] can have further clinical implications because oligodendroglioma tend to be more circumscribed and respond better to chemotherapy than astrocytoma [117]. In contrast, the astrocytoma diffusely infiltrates the surrounding normal brain, and has greater tendency to progress to a more malignant histological type, and is more resistant to chemotherapy.

The *in vivo* TRFS studies of HGG [32], [33] demonstrated that this brain tumor group is characterized by a broad range of fluorescence emission characteristics. Both spectral and temporal emission profiles appeared to vary not only with tumor phenotype (e.g., GBM and anaplastic oligodendroglioma), as observed for LGG, but also with the location within tumor from where the data were recorded. It was noted that HGG tumors are highly heterogeneous and in many instances the spectroscopic characteristics retrieved from the center of the tumor are very different from those obtained from the tumor margins (see Fig. 4). In addition to the main peak emission at 460 nm, HGG consistently presented an additional peak emission centered at about 380–390 nm, similar to that observed for NC and NWM. This peak was associated with two fluorophores known to emit fluorescence within this wavelength band, PMP and GAD [118]. Both of these fluorophores are metabolically affected in gliomas. Overall, the fluorescence lifetime of HGG was found longer (e.g., >1 ns at 460 nm) than that of LLG. Discrimination between HGG tissue and normal brain tissue relied on the use of Laguerre coefficients that provided a more accurate representation of the fluorescence decay dynamics than the conventional average fluorescence lifetime parameter. Measurements conducted in a recurrent glioma with radiation necrosis also demonstrated very distinctive characteristics. Specifically, the tumor displayed a single emission peak at 390 nm suggesting the emission of fibrotic constituents.

A linear discriminant algorithm [33] also demonstrated that a combination of spectroscopic parameters derived from both spectral and temporal domains enables the classification of LGG with 100% sensitivity and 98% specificity and that of HGG with 47% sensitivity and 94% specificity. The low sensitivity obtained for HGG was attributed to the high degree of heterogeneity of these tumors.

Differences between *in vivo* and *ex vivo* TRFS measurements of brain tumors were also reported [32]. Although the exact cause of such differences is still to be elucidated, it has been suggested that such changes are due to differences in the environment and/or metabolic changes that may occur after tissue excision.

B. FLIM of Glioma

The first application of a FLIM technique to intraoperative delineation of brain tumor margins has been also recently reported [34]. A pilot study employing the prototype FLIM apparatus described earlier was conducted in three patients (13 sites) diagnosed with HGG (GBM). This study evaluated whether the fluorescence lifetime contrast can be achieved between normal brain and brain tumor areas as identified by diagnostic methods typically used during neurosurgical procedures (preoperative MRI images and neurosurgeon experience). Since the time-resolved images are minimally affected by factors that often confound point spectroscopic analysis, including irregular tissue surfaces, nonuniform illumination, and endogenous absorbers such as blood in the operative field, FLIM was considered particularly appropriate for intraoperative use. A bandpass filter with a center wavelength of 460 nm and a bandwidth of 50 nm corresponding to NAD(P)H fluorescence was used in this study. Data acquisition time for each measurement was ~2 min, including one steady-state image and a series of up to 29 time-gated images (0.5 ns gating time and 0.5 ns relative delay-time interval). During imaging, the probe was gently positioned perpendicular to the tissue surface and held with a Greenberg device to minimize movement artifacts (see Fig. 2).

Results from this FLIM study (see Fig. 5) concurred with those reported for TRFS measurements. They underscored that fluorescence lifetime contrast generated by the relative changes in free/bound NAD(P)H conditions plays an important role in the delineation of tumor from normal surrounding tissue. These changes resulted in a slightly longer fluorescence lifetime for GBM (~1.6 ns) when compared with NC (~1.3 ns). Important for clinical applications, this study also demonstrated that fluorescence lifetime contrast between tumor and normal tissue can be consistently achieved and is independent of tissue illumination, irregular brain tissue surface, and presence of blood in the surgical field [34].

V. Conclusion

Over the past decade, a few techniques based on endogenous fluorescence contrast have demonstrated potential for diagnosis of primary brain tumors in patients, tumor demarcation, and surgical guidance [25]–[27], [30]–[35], [91], [92]. This approach has intrinsic advantages for a fast translation of diagnostic and image-guided surgery devices to the clinical environment since they do not require administration of contrast agents and thus can

circumvent potential medical complications. However, the number of studies concerning this approach is few and no systematic clinical trial was conducted or reported to date. Instrumentation employing time-resolved fluorescence measurement methods, as reviewed in this paper, was shown to improve the specificity of fluorescence measurement [30]–[35].

Clinical implementation of both point spectroscopy (TRFS) and imaging (FLIM) techniques demonstrated the utility of fluorescence contrast for characterization and diagnosis of brain tumors. However, their full capabilities as adjunct tools in neurosurgery have been underexplored. Challenges and opportunities for a more effective evaluation of these techniques in clinical settings are outlined next.

First, time-resolved fluorescence techniques have demonstrated potential for detecting subtle changes in fluorescence signatures as a function of tumor phenotype and histopathologic subclassification [33], a capability that may help in determining the prognosis of the surgical treatment. If the diagnosis can be made during the tumor excision, then the autofluorescence signatures may potentially be useful in determining the course of therapy. A complete analysis of this capability, however, would require a systematic study of fluorescence signatures as a function of both biological diversity, heterogeneities in both LGG and HGG brain tumors, and intrapatient signature variability. This would require not only enrolment of a large number of patients but also a rigorous correlation of fluorescence signatures with the histopathology of the biochemical characterization of the optically interrogated tissue. This, in particular, is challenging since only a limited number of biopsies can be obtained from one patient undergoing surgery for removal of brain tumor. New strategies need to be developed in order to support a rapid and systematic validation of the optical technologies.

Second, time-resolved measurements are less sensitive to variations in fluorescence excitation–collection geometry and presence of endogenous absorbers. Both TRFS and FLIM studies conducted in patients have underscored this important feature that supports their clinical compatibility. For example, despite nonuniform illumination of tissue surface, robust fluorescence lifetime values can be obtained from FLIM images. Also, analysis of fluorescence data obtained from brain surfaces subject to moving artifacts (arterial pulsation, breathing, etc.) [32] demonstrated that such artifacts affect the spectral emission profile but not fluorescence lifetime values. Enhancing the SNR, however, is important for improved detection sensitivity and reducing the time of data acquisition. Methods that maximize the photon collection efficiency and minimize the interference of biological fluids with optical signals will be important for future work.

Third, the endogenous fluorescence-based techniques have the inherent capability of providing real-time diagnostic information. Nevertheless, this relies on the design of TRFS or FLIM devices that allows for fast data acquisition, online data processing, and display of diagnostic information. The TRFS and FLIM instruments used in patients required ~30 s for the acquisition of a point dataset and ~2 min for the acquisition of a time-resolved image, respectively. While these devices were useful in demonstrating the initial feasibility of these techniques to operate in the clinical environment, they are not fully suitable for large clinical research trials. New methods recently reported [36], [37] allow for fast acquisition (<1 μs) of time-resolved fluorescence data in multiple spectral bands simultaneously and have the

potential to overcome such challenges. However, implementation of these devices in neurosurgery needs to be explored in future work. Development of computational models based on the Laguerre deconvolution technique also enabled fast processing (<1 s) of multiple fluorescence decay profiles [107], [110]. Such methods are likely to address the need for online data processing. Yet, the ability to classify and diagnose tumors in real time will depend on the ability to generate a large training database of time-resolved florescence emission features correlated with tumor distinct histopathologic features. Since the brain tumor fluorescence emission features change post tissue excision, such a database would need to be generated based on features obtained from *in vivo* measurements in human patients.

Acknowledgments

The fluorescence lifetime studies in patients summarized in this paper were conducted in collaboration with the Maxine–Dunitz Neurosurgical Institute at Cedars Sinai Medical Center and the Department of Neurological Surgery at the University of California Davis Medical Center. The authors acknowledge the contribution to this work of Dr. P. Butte and clinical collaborators Dr. K. L. Black, Dr. B. K. Pikul, Dr. A. N. Mamelak, Dr. R. C. Thompson, Dr. W. H. Yong, and Dr. S. I. Bannykh at Cedars-Sinai and Dr. R. Schrot and F. Gorin at UC Davis.

This work was supported in part by the National Institutes of Health under Grant R42 CA117286 and in part by the Cancer Center at the University of California Davis.

Biographies

Laura Marcu received the M.S. and Ph.D. degrees in biomedical engineering from the University of Southern California, Los Angeles, in 1995 and 1998, respectively.

From 2002 to 2005, she was a Research Scientist and Director of the Biophotonics Research and Technology Development Laboratory, Department of Surgery, Cedars-Sinai Medical Center, Los Angeles. From 2000 to 2005, she was also an Assistant and Associate Professor of biomedical engineering and electrical engineering-electrophysics, University of Southern California. In 2006, she joined the University of California, Davis, where she is currently a Professor of biomedical engineering and neurological surgery and directs research in the area of biomedical optics with applications in cardiology, oncology, and tissue engineering.

Dr. Marcu became a Fellow (elected) of the Biomedical Engineering Society in 2011 and the American Institute for Medical and Biological Engineering in 2010.

Brad A. Hartl received the B.S. degree in physics with biomedical concentration from the University of Wisconsin-La Crosse, La Crosse, WI, in 2009. He is currently working toward the M.S. degree in biomedical engineering from the University of California, Davis.

References

1. (2011, Sep. 2). [Online]. Available: www.cancer.gov/cancertopics/types/brain
2. (2011, Sep. 16). [Online]. Available: www.cancer.gov/aboutnci/servingpeople/snapshots/brain.pdf
3. (2011, Sep. 2). [Online]. Available: www.cbtrus.org/reports/2007-2008/2007report.pdf
4. Louis DN, Ohgaki H, Wiestler OD, Cavenee WK, Burger PC, Jouvet A, Scheithauer BW, Kleihues P. The 2007 WHO classification of tumours of the central nervous system. Acta Neuropathol. Aug. 2007 114:97–109. [PubMed: 17618441]

5. Wen PY, Kesari S. Malignant gliomas in adults. N Engl J Med. 2008; 359:492–507. [PubMed: 18669428]
6. Robins HI, Lassman AB, Khuntia D. Therapeutic advances in malignant glioma: Current status and future prospects. Neuroimag Clin N Amer. Nov.2009 19:647–656.
7. Stummer W, Reulen HJ, Meinel T, Pichlmeier U, Schumacher W, Tonn JC, Rohde V, Oppel F, Turowski B, Woiciechowsky C, Franz K, Pietsch T, Grp A-GS. Extent of resection and survival on glioblastoma multiforme-identification of and adiustment for bias. Neurosurgery. Mar.2008 62:564–574. [PubMed: 18425006]
8. Sanai N, Berger MS. Glioma extent of resection and its impact on patient outcome. Neurosurgery. Apr.2008 62:753–764. [PubMed: 18496181]
9. Lacroix M, Abi-Said D, Fourney DR, Gokaslan ZL, Shi W, DeMonte F, Lang FF, McCutcheon IE, Hassenbusch SJ, Holland E, Hess K, Michael C, Miller D, Sawaya R. A multivariate analysis of 416 patients with glioblastoma multiforme: Prognosis, extent of resection, and survival. J Neurosurg. Aug.2001 95:190–198.
10. Lunsford LD, Niranjan A, Kassam A, Khan A, Amin D, Kondziolka D. Intraoperative imaging: Evolutions, options, and practical applications. Clin Neurosurg. 2008; 55:76–86. [PubMed: 19248671]
11. Elias WJ, Fu KM, Frysinger RC. Cortical and subcortical brain shift during stereotactic procedures. J Neurosurg. Nov.2007 107:983–988. [PubMed: 17977271]
12. Sohn, C.; Voigt, HJ.; Vetter, K. Doppler Ultrasound in Gynecology and Obstetrics. New York, NY: Thieme; 2004.
13. Toms SA, Grosu ID, Toms MA. Nanoimaging and neurological surgery. WIREs, Nanomed Nanobiotechnol. Nov-Dec;2010 2:601–617.
14. Comeau RM, Sadikot AF, Fenster A, Peters TM. Intraoperative ultrasound for guidance and tissue shift correction in image-guided neurosurgery. Med Phys. Apr.2000 27:787–800. [PubMed: 10798702]
15. Bucholz, R.; Yeh, D.; Trobaugh, J.; McDurmont, L.; Sturm, C.; Baumann, C.; Henderson, J.; Levy, A.; Kessman, P. CVRMed-MRCAS'97. Vol. 1205. Berlin/Heidelberg, Germany: Springer; 1997. The correction of stereotactic inaccuracy caused by brain shift using an intraoperative ultrasound device; p. 459-466.
16. Unsgaard G, Ommedal S, Muller T, Gronningsaeter A, Nagelhus Hernes TA. Neuronavigation by intraoperative three-dimensional ultrasound: initial experience during brain tumor resection. Neurosurgery. 2002; 50:804–812. [PubMed: 11904032]
17. Unsgaard G, Gronningsaeter A, Ommedal S, Nagelhus Hernes TA. Brain operations guided by real-time two-dimensional ultrasound: New possibilities as a result of improved image quality. Neurosurgery. Aug.2002 51:402–411. discussion 411–412. [PubMed: 12182778]
18. Kubben PL, Ter Meulen KJ, Schijns OE, Ter Laak-Poort MP, van Overbeeke JJ, Santbrink H. Intraoperative MRI-guided resection of glioblastoma multiforme: A systematic review. Lancet Oncol. Oct.2011 12:1062–1070. [PubMed: 21868286]
19. Senft C, Bink A, Franz K, Vatter H, Gasser T, Seifert V. Intraoperative MRI guidance and extent of resection in glioma surgery: A randomised, controlled trial. Lancet Oncol. Oct.2011 12:997–1003. [PubMed: 21868284]
20. Hall WA, Truwit CL. Intraoperative MR-guided neurosurgery. J Magn Reson Imag. 2008; 27:368–375.
21. Lewin JS, Metzger A, Selman WR. Intraoperative magnetic resonance image guidance in neurosurgery. J Magn Reson Imag. 2000; 12:512–524.
22. Kostron H. Photodynamic diagnosis and therapy and the brain. Methods Mol Biol. 2010; 635:261–280. [PubMed: 20552352]
23. Kostron H, Fiegele T, Akatuna E. Combination of FOSCAN® mediated fluorescence guided resection and photodynamic treatment as new therapeutic concept for malignant brain tumors. Med Laser Appl. 2006; 21:285–290.
24. Pogue BW, Gibbs-Strauss S, Valdes PA, Samkoe K, Roberts DW, Paulsen KD. Review of neurosurgical fluorescence imaging methodologies. IEEE J Sel Top Quantum Electron. Nov-Dec; 2010 16:1847–1847.

25. Lin WC, Toms SA, Johnson M, Jansen ED, Mahadevan-Jansen A. In vivo brain tumor demarcation using optical spectroscopy. Photochem Photobiol. Apr.2001 73:396–402. [PubMed: 11332035]
26. Toms SA, Lin WC, Weil RJ, Johnson MD, Jansen ED, Mahadevan-Jansen A. Intraoperative optical spectroscopy identifies infiltrating glioma margins with high sensitivity. Neurosurgery. Oct.2005 57:382–391. [PubMed: 16234690]
27. Lin WC, Mahadevan-Jansen A, Johnson MD, Weil RJ, Toms SA. In vivo optical spectroscopy detects radiation damage in brain tissue. Neurosurgery. Sep.2005 57:518–525. [PubMed: 16145531]
28. Gebhart SC, Thompson RC, Mahadevan-Jansen A. Liquid-crystal tunable filter spectral imaging for brain tumor demarcation. Appl Opt. Apr 1.2007 46:1896–1910. [PubMed: 17356636]
29. Fang QY, Papaioannou T, Jo JA, Vaitha R, Shastry K, Marcu L. Time-domain laser-induced fluorescence spectroscopy apparatus for clinical diagnostics. Rev Sci Instrum. Jan.2004 75:151–162.
30. Marcu L, Jo JA, Butte PV, Yong WH, Pikul BK, Black KL, Thompson RC. Fluorescence lifetime spectroscopy of glioblastoma multiforme. Photochem Photobiol. Jul-Aug;2004 80:98–103. [PubMed: 15339216]
31. Yong WH, Butte PV, Pikul BK, Jo JA, Fang QY, Papaioannou T, Black KL, Marcu L. Distinction of brain tissue, low grade and high grade glioma with time-resolved fluorescence spectroscopy. Front Biosci. May 1.2006 11:1255–1263. [PubMed: 16368511]
32. Butte PV, Fang Q, Jo JA, Yong WH, Pikul BK, Black KL, Marcu L. Intraoperative delineation of primary brain tumors using time-resolved fluorescence spectroscopy. J Biomed Opt. Mar-Apr; 2010 15:027008-1–027008-8. [PubMed: 20459282]
33. Butte PV, Mamelak AN, Nuno M, Bannykh SI, Black KL, Marcu L. Fluorescence lifetime spectroscopy for guided therapy of brain tumors. Neuroimage. Jan; 2011 54(Suppl 1):S125–S135. [PubMed: 21055475]
34. Sun Y, Hatami N, Yee M, Phipps J, Elson DS, Gorin F, Schrot RJ, Marcu L. Fluorescence lifetime imaging microscopy for brain tumor image-guided surgery. J Biomed Opt. 2010; 15:056022. [PubMed: 21054116]
35. Butte PV, Pikul BK, Hever A, Yong WH, Black KL, Marcu L. Diagnosis of meningioma by time-resolved fluorescence spectroscopy. J Biomed Opt. Nov-Dec;2005 10:064026-1–064026-8. [PubMed: 16409091]
36. Sun Y, Stephens D, Xie H, Phipps J, Saroufeem R, Southard J, Elson DS, Marcu L. Dynamic tissue analysis using time- and wavelength-resolved fluorescence spectroscopy for atherosclerosis diagnosis. Opt Express. Feb 28.2011 19:3890–3901. [PubMed: 21369214]
37. Sun Y, Chaudhari AJ, Lam M, Xie H, Yankelevich DR, Phipps J, Liu J, Fishbein MC, Cannata JM, Shung KK, Marcu L. Multimodal characterization of compositional, structural and functional features of human atherosclerotic plaques. Biomed Opt Express. Aug.2011 2:2288–2298. [PubMed: 21833365]
38. Sosna J, Barth MM, Kruskal JB, Kane RA. Intraoperative sonography for neurosurgery. J Ultrasound Med. Dec.2005 24:1671–1682. [PubMed: 16301724]
39. Unsgaard G, Rygh OM, Selbekk T, Muller TB, Kolstad F, Lindseth F, Hernes TA. Intra-operative 3D ultrasound in neurosurgery. Acta Neurochir (Wien). Mar.2006 148:235–253. [PubMed: 16362178]
40. Regelsberger J, Lohmann F, Helmke K, Westphal M. Ultrasound-guided surgery of deep seated brain lesions. Eur J Ultrasound. Dec.2000 12:115–121. [PubMed: 11118918]
41. Nabavi A, Black PM, Gering DT, Westin CF, Mehta V, Pergolizzi RS Jr, Ferrant M, Warfield SK, Hata N, Schwartz RB, Wells WM 3rd, Kikinis R, Jolesz FA. Serial intraoperative magnetic resonance imaging of brain shift. Neurosurgery. Apr.2001 48:787–798. [PubMed: 11322439]
42. Hadani M, Spiegelman R, Feldman Z, Berkenstadt H, Ram Z. Novel, compact, intraoperative magnetic resonance imaging-guided system for conventional neurosurgical operating rooms. Neurosurgery. Apr.2001 48:799–809. [PubMed: 11322440]
43. Black PM, Alexander E 3rd, Martin C, Moriarty T, Nabavi A, Wong TZ, Schwartz RB, Jolesz F. Craniotomy for tumor treatment in an intraoperative magnetic resonance imaging unit. Neurosurgery. Sep.1999 45:423–433. [PubMed: 10493363]

44. Foroglou N, Zamani A, Black P. Intra-operative MRI (iop-MR) for brain tumour surgery. Br J Neurosurg. Feb.2009 23:14–22. [PubMed: 19234904]
45. Senft C, Seifert V, Hermann E, Franz K, Gasser T. Usefulness of intraoperative ultra low-field magnetic resonance imaging in glioma surgery. Neurosurgery. 2008; 63:257–267. [PubMed: 18981831]
46. Knauth M, Aras N, Wirtz CR, Dorfler A, Engelhorn T, Sartor K. Surgically induced intracranial contrast enhancement: Potential source of diagnostic error in intraoperative MR imaging. Amer J Neuroradiol. Sep.1999 20:1547–1553. [PubMed: 10512244]
47. Fahlbusch R, Ganslandt O, Nimsky C. Intraoperative imaging with open magnetic resonance imaging and neuronavigation. Childs Nerv Syst. Nov.2000 16:829–831. [PubMed: 11151737]
48. Schneider JP, Schulz T, Schmidt F, Dietrich J, Lieberenz S, Trantakis C, Seifert V, Kellermann S, Schober R, Schaffranietz L, Laufer M, Kahn T. Gross-total surgery of supratentorial low-grade gliomas under intraoperative MR guidance. Amer J Neuroradiol. Jan.2001 22:89–98. [PubMed: 11158893]
49. Maeda H, Iyer AK, Khaled G, Fang J. Exploiting the enhanced permeability and retention effect for tumor targeting. Drug Discov Today. Sep.2006 11:812–818. [PubMed: 16935749]
50. Moore GE, Peyton WT, French LA, Walker WW. The clinical use of fluorescein in neurosurgery—The localization of brain tumors. J Neurosurg. 1948; 5:392–398. [PubMed: 18872412]
51. Kremer P, Mahmoudreza F, Ding R, Pritsch M, Zoubaa S, Frei E. Intraoperative fluorescence staining of malignant brain tumors using 5-aminofluorescein-labeled albumin. Neurosurgery. Mar. 2009 64:S53–S61.
52. Shinoda J, Yano H, Yoshimura SI, Okumura A, Kaku Y, Iwama T, Sakai N. Fluorescence-guided resection of glioblastoma multiforme, by using high-dose fluorescein sodium - Technical note. J Neurosurg. Sep.2003 99:597–603. [PubMed: 12959452]
53. Kuroiwa T, Kajimoto Y, Ohta T. Comparison between operative findings on malignant glioma by a fluorescein surgical microscopy and histological findings. Neurol Res. Jan.1999 21:130–134. [PubMed: 10048072]
54. Okuda T, Kataoka K, Yabuuchi T, Yugami H, Kato A. Fluorescence-guided surgery of metastatic brain tumors using fluorescein sodium. J Clin Neurosci. Jan.2010 17:118–121. [PubMed: 19969462]
55. Sato S, Toya S, Otani M. Blood-brain barrier opening microcirculation in human brain tumor. No To Shinkei. Feb.1985 37:109–113. [PubMed: 2988587]
56. Haglund MM, Berger MS, Hochman DW. Enhanced optical imaging of human gliomas and tumor margins. Neurosurgery. 1996; 38:308–317. [PubMed: 8869058]
57. Chang JH, Kim EH, Cho JM, Kim SH, Lee KS. Application of intraoperative indocyanine green videoangiography to brain tumor surgery. Acta Neurochir (Wien). Jul.2011 153:1487–1495. [PubMed: 21590519]
58. Ferroli P, Acerbi F, Albanese E, Tringali G, Broggi M, Franzini A, Broggi G. Application of intraoperative indocyanine green angiography for CNS tumors: Results on the first 100 cases. Acta Neurochir Suppl. 2011; 109:251–257. [PubMed: 20960352]
59. Cherrick GR, Stein SW, Leevy CM, Davidson CS. Indocyanine green: Observations on its physical properties, plasma decay, and hepatic extraction. J Clin Invest. 1960; 39:592–600. [PubMed: 13809697]
60. Desmettre T, Devoisselle JM, Mordon S. Fluorescence properties and metabolic features of indocyanine green (ICG) as related to angiography. Surv Ophthalmol. Jul-Aug;2000 45:15–27. [PubMed: 10946079]
61. Zimmermann A, Ritsch-Marte M, Kostron H. mTHPC-mediated photodynamic diagnosis of malignant brain tumors. Photochem Photobiol. Oct.2001 74:611–616. [PubMed: 11683042]
62. Kostron H, Zimmermann A, Obwegeser A. mTHPC-mediated photodynamic detection for fluorescence-guided resection of brain tumors. Proc SPIE. 1998; 3262:259–264.
63. Eljamel MS, Goodman C, Moseley H. ALA and Photofrin (R) fluorescence-guided resection and repetitive PDT in glioblastoma multiforme: A single centre Phase III randomised controlled trial. Lasers Med Sci. Oct.2008 23:361–367. [PubMed: 17926079]

64. Lilge L, Olivo MC, Schatz SW, MaGuire JA, Patterson MS, Wilson BC. The sensitivity of normal brain and intracranially implanted VX2 tumour to interstitial photodynamic therapy. Br J Cancer. Feb.1996 73:332–343. [PubMed: 8562339]
65. Stummer W, Stocker S, Novotny A, Heimann A, Sauer O, Kempski O, Plesnila N, Wietzorrek J, Reulen HJ. In vitro and in vivo porphyrin accumulation by C6 glioma cells after exposure to 5-aminolevulinic acid. J Photochem Photobiol B. Sep.1998 45:160–169. [PubMed: 9868806]
66. Muller, PJABCW. Photodynamic therapy for brain tumours. In: McCaughan, J., editor. Photodynamic Therapy of Malignancies. Austin, TX: Landes; 1993. p. 201-211.
67. Muller PJ, Wilson BC. Photodynamic therapy for recurrent supratentorial gliomas. Semin Surg Oncol. Sep-Oct;1995 11:346–354. [PubMed: 7569556]
68. Kaye AH, Hill JS. Photodynamic therapy of brain tumours. Ann Acad Med Singapore. May.1993 22:470–481. [PubMed: 8215203]
69. Collaud S, Juzeniene A, Moan J, Lange N. On the selectivity of 5-aminolevulinic acid-induced protoporphyrin IX formation. Curr Med Chem Anticancer Agents. May.2004 4:301–316. [PubMed: 15134506]
70. Friesen SA, Hjortland GO, Madsen SJ, Hirschberg H, Engebraten O, Nesland JM, Peng Q. 5-Aminolevulinic acid-based photodynamic detection and therapy of brain tumors (review). Int J Oncol. Sep.2002 21:577–582. [PubMed: 12168102]
71. Peng Q, Warloe T, Berg K, Moan J, Kongshaug M, Giercksky KE, Nesland JM. 5-aminolevulinic acid-based photodynamic therapy. Clinical research and future challenges. Cancer. 1997; 79:2282–2308. [PubMed: 9191516]
72. Wilson BC, Bogaards A, Varma A, Collens SP, Lin AH, Giles A, Yang VXD, Bilbao JM, Lilge LD, Muller PJ. Increased brain tumor resection using fluorescence image guidance in a preclinical model. Lasers Surg Med. 2004; 35:181–190. [PubMed: 15389738]
73. Olivo M, Wilson BC. Mapping ALA-induced PPIX fluorescence in normal brain and brain tumour using confocal fluorescence microscopy. Int J Oncol. Jul.2004 25:37–45. [PubMed: 15201987]
74. Stummer W, Pichlmeier U, Meinel T, Wiestler OD, Zanella F, Hans-Jurgen R, Grp A-GS. Fluorescence-guided surgery with 5-aminolevulinic acid for resection of malignant glioma: A randomised controlled multicentre phase III trial. Lancet Oncol. May.2006 7:392–401. [PubMed: 16648043]
75. Stummer W, Novotny A, Stepp H, Goetz C, Bise K, Reulen HJ. Fluorescence-guided resection of glioblastoma multiforme by using 5-aminolevulinic acid-induced porphyrins: A prospective study in 52 consecutive patients. J Neurosurg. Dec.2000 93:1003–1013. [PubMed: 11117842]
76. Stummer W, Stocker S, Wagner S, Stepp H, Fritsch C, Goetz C, Goetz AE, Kiefmann R, Reulen HJ. Intraoperative detection of malignant gliomas by 5-aminolevulinic acid-induced porphyrin fluorescence. Neurosurgery. Mar.1998 42:518–525. discussion 525–526. [PubMed: 9526986]
77. Stummer W, Pichlmeier U, Bink A, Schackert G, Grp AGS. Resection and survival in glioblastoma multiforme: An RTOG recursive partitioning analysis of ALA study patients. Neuro-oncol. Dec. 2008 10:1025–1034. [PubMed: 18667747]
78. Tamura Y, Kuroiwa T, Kajimoto Y, Miki Y, Miyatake SI, Tsuji M. Endoscopic identification and biopsy sampling of an intraventricular malignant glioma using a 5-aminolevulinic acid-induced protoporphyrin IX fluorescence imaging system. Technical note. J Neurosurg. Mar.2007 106:507–510. [PubMed: 17367078]
79. Utsuki S, Oka H, Sato S, Shimizu S, Suzuki S, Tanizaki Y, Kondo K, Miyajima Y, Fujii K. Histological examination of false positive tissue resection using 5-aminolevulinic acid-induced fluorescence guidance. Neurol Med Chir (Tokyo). May.2007 47:210–213. [PubMed: 17527047]
80. Toda M. Intraoperative navigation and fluorescence imagings in malignant glioma surgery. Keio J Med. Sep.2008 57:155–161. [PubMed: 18854668]
81. Kajimoto Y, Kuroiwa T, Miyatake SI, Ichioka T, Miyashita M, Tanaka H, Tsuji M. Use of 5-aminolevulinic acid in fluorescence-guided resection of meningioma with high risk of recurrence —Case report. J Neurosurg. Jun.2007 106:1070–1074. [PubMed: 17564181]
82. Miyatake S, Kuroiwa T, Kajimoto Y, Miyashita M, Tanaka H, Tsuji M. Fluorescence of non-neoplastic, magnetic resonance imaging-enhancing tissue by 5-aminolevulinic acid: Case report. Neurosurgery. Nov.2007 61:E1101–E1104. [PubMed: 18091261]

83. Morofuji Y, Matsuo T, Hayashi Y, Suyama K, Nagata I. Usefulness of intraoperative photodynamic diagnosis using 5-aminolevulinic acid for meningiomas with cranial invasion: Technical case report. Neurosurgery. 2008; 62:102–104. [PubMed: 18424972]
84. Hefti M, Campe GV, Moschopulosa M, Siegnerb A, Looserc H, Landolt H. 5-aminolaevulinic acid-induced protoporphyrin IX fluorescence in high-grade glioma surgery. Swiss Med Wkly. 2008; 138:180–185. [PubMed: 18363116]
85. Leblond F, Fontaine KM, Valdes P, Ji S, Pogue BW, Hartov A, Roberts DW, Paulsen KD. Brain tumor resection guided by fluorescence imaging. Proc SPIE. 2009; 7164:71640M-1–71640M-8.
86. Ishihara R, Katayama Y, Watanabe T, Yoshino A, Fukushima T, Sakatani K. Quantitative spectroscopic analysis of 5-aminolevulinic acid-induced protoporphyrin IX fluorescence intensity in diffusely infiltrating astrocytomas. Neurol Med Chir (Tokyo). Feb.2007 47:53–57. [PubMed: 17317941]
87. Utsuki S, Oka H, Miyajima Y, Shimizu S, Suzuki S, Fujii K. Auditory alert system for fluorescence-guided resection of gliomas. Neurol Med Chir (Tokyo). Feb.2008 48:95–98. [PubMed: 18296881]
88. Utsuki S, Oka H, Sato S, Suzuki S, Shimizu S, Tanaka S, Fujii K. Possibility of using laser spectroscopy for the intraoperative detection of nonfluorescing brain tumors and the boundaries of brain tumor infiltrates. Technical note. J Neurosurg. Apr.2006 104:618–620. [PubMed: 16619668]
89. Yang VX, Muller PJ, Herman P, Wilson BC. A multispectral fluorescence imaging system: Design and initial clinical tests in intraoperative Photofrin-photodynamic therapy of brain tumors. Lasers Surg Med. 2003; 32:224–232. [PubMed: 12605430]
90. Stummer W, Stepp H, M??ller G, Ehrhardt A, Leonhard M, Reulen HJ. Technical principles for protoporphyrin-IX-fluorescence guided microsurgical resection of malignant glioma tissue. Acta Neurochir (Wien). 1998; 140:995–1000. [PubMed: 9856241]
91. Croce AC, Fiorani S, Locatelli D, Nano R, Ceroni M, Tancioni F, Giombelli E, Benericetti E, Bottiroli G. Diagnostic potential of autofluorescence for an assisted intraoperative delineation of glioblastoma resection margins. Photochem Photobiol. Mar.2003 77:309–318. [PubMed: 12685660]
92. Bottiroli G, Croce AC, Locatelli D, Nano R, Giombelli E, Messina A, Benericetti E. Brain tissue autofluorescence: an aid for intraoperative delineation of tumor resection margins. Cancer Detect Prev. 1998; 22:330–339. [PubMed: 9674876]
93. Lakowicz JR, Szmacinski H, Nowaczyk K, Johnson ML. Fluorescence lifetime imaging of free and protein-bound NADH. Proc Nat Acad Sci USA. 1992; 89:1271–1275. [PubMed: 1741380]
94. Yan H, Parsons DW, Jin G, McLendon R, Rasheed BA, Yuan W, Kos I, Batinic-Haberle I, Jones S, Riggins GJ, Friedman H, Friedman A, Reardon D, Herndon J, Kinzler KW, Velculescu VE, Vogelstein B, Bigner DD. IDH1 and IDH2 mutations in gliomas. N Engl J Med. Feb 19.2009 360:765–773. [PubMed: 19228619]
95. Lakowicz, JR. Principles of Fluorescence Spectroscopy. New York: Springer; 2006.
96. Mycek, MA.; Pogue, BW. Handbook of Biomedical Fluorescence. Boca Raton, FL: CRC Press; 2003.
97. Elson, D.; Galletly, N.; Talbot, C.; Requejo-Isidro, J.; McGinty, J.; Dunsby, C.; Lanigan, P.; Munro, I.; Benninger, R.; Beule, P.; Auksorius, E.; Hegyi, L.; Sandison, A.; Wallace, A.; Soutter, P.; Neil, M.; Lever, J.; Stamp, G.; French, P. Multidimensional fluorescence imaging applied to biological tissue. In: Geddes, C.; Lakowicz, J., editors. Reviews in Fluorescence. Vol. 2006. New York: Springer; 2006. p. 477-524.
98. Chorvat D, Chorvatova A. Multi-wavelength fluorescence lifetime spectroscopy: A new approach to the study of endogenous fluorescence in living cells and tissues. Laser Phys Lett. Mar.2009 6:175–193.
99. Cubeddu R, Comelli D, D'Andrea C, Taroni P, Valentini G. Time-resolved fluorescence imaging in biology and medicine. J Phys D. May.2002 35:R61–R76.
100. Mizeret J, Wagnieres G, Stepinac T, VandenBergh H. Endoscopic tissue characterization by frequency-domain fluorescence lifetime imaging (FD-FLIM). Lasers Med Sci. 1997; 12:209–217. [PubMed: 20803328]

101. Pfefer TJ, Paithankar DY, Poneros JM, Schomacker KT, Nishioka NS. Temporally and spectrally resolved fluorescence spectroscopy for the detection of high grade dysplasia in Barrett's esophagus. Lasers Surg Med. 2003; 32:10–16. [PubMed: 12516065]
102. Pitts JD, Mycek MA. Design and development of a rapid acquisition laser-based fluorometer with simultaneous spectral and temporal resolution. Rev Sci Instrum. Jul.2001 72:3061–3072.
103. Sun Y, Park J, Stephens DN, Jo JA, Sun L, Cannata JM, Saroufeem RM, Shung KK, Marcu L. Development of a dual-modal tissue diagnostic system combining time-resolved fluorescence spectroscopy and ultrasonic backscatter microscopy. Rev Sci Instrum. Jun.2009 80:065104. [PubMed: 19566223]
104. Sun Y, Phipps J, Elson DS, Stoy H, Tinling S, Meier J, Poirier B, Chuang FS, Farwell DG, Marcu L. Fluorescence lifetime imaging microscopy: in vivo application to diagnosis of oral carcinoma. Opt Lett. Jul 1.2009 34:2081–2083. [PubMed: 19572006]
105. Elson DS, Jo JA, Marcu L. Miniaturized side-viewing imaging probe for fluorescence lifetime imaging (FLIM): Validation with fluorescence dyes, tissue structural proteins and tissue specimens. New J Phys. May.2007 9:1–11.
106. McGinty J, Galletly NP, Dunsby C, Munro I, Elson DS, Requejo-Isidro J, Cohen P, Ahmad R, Forsyth A, Thillainayagam AV, Neil MA, French PM, Stamp GW. Wide-field fluorescence lifetime imaging of cancer. Biomed Opt Express. 2010; 1:627–640. [PubMed: 21258496]
107. Jo JA, Fang QY, Papaioannou T, Marcu L. Fast model-free deconvolution of fluorescence decay for analysis of biological systems. J Biomed Opt. Jul-Aug;2004 9:743–752. [PubMed: 15250761]
108. Ware WR, Doemeny LJ, Nemzek TL. Deconvolution of fluorescence and phosphorescence decay curves. Least-squares method. J Phys Chem. 1973; 77:2038–2048.
109. Oconnor DV, Ware WR, Andre JC. Deconvolution of fluorescence decay curves. A critical comparison of techniques. J Phys Chem. 1979; 83:1333–1343.
110. Jo JA, Fang Q, Papaioannou T, Baker JD, Dorafshar AH, Reil T, Qiao JH, Fishbein MC, Freischlag JA, Marcu L. Laguerre-based method for analysis of time-resolved fluorescence data: Application to in-vivo characterization and diagnosis of atherosclerotic lesions. J Biomed Opt. Mar-Apr;2006 11:021004-1–021004-13. [PubMed: 16674179]
111. Marcu L, Fishbein MC, Maarek JMI, Grundfest WS. Discrimination of human coronary artery atherosclerotic lipid-rich lesions by time-resolved laser-induced fluorescence spectroscopy. Arterioscler Thromb Vasc Biol. 2001; 21:1244–1250. [PubMed: 11451759]
112. Marcu L, Jo JA, Fang QY, Papaioannou T, Reil T, Qiao JH, Baker JD, Freischlag JA, Fishbein MC. Detection of rupture-prone atherosclerotic plaques by time-resolved laser-induced fluorescence spectroscopy. Atherosclerosis. May.2009 204:156–1164. [PubMed: 18926540]
113. Ng HK, Wong ATC. Expression of epithelial and extracellular-matrix protein markers in meningiomas. Histopathology. Feb.1993 22:113–125. [PubMed: 7681027]
114. Nitta H, Yamashima T, Yamashita J, Kubota T. An ultrastructural and immunohistochemical study of extracellular-matrix in meningiomas. Histol Histopathol. 1990; 5:267–274. [PubMed: 2134380]
115. Gill SS, Thomas DG, Van Bruggen N, Gadian DG, Peden CJ, Bell JD, Cox IJ, Menon DK, Iles RA, Bryant DJ, et al. Proton MR spectroscopy of intracranial tumours: In vivo and in vitro studies. J Comput Assist Tomogr. Jul-Aug;1990 14:497–504. [PubMed: 2164536]
116. Sell DR, Monnier VM. Isolation, purification and partial characterization of novel fluorophores from aging human insoluble collagen-rich tissue. Connect Tissue Res. 1989; 19:77–92. [PubMed: 2791558]
117. Watanabe T, Nakamura M, Kros JM, Burkhard C, Yonekawa Y, Kleihues P, Ohgaki H. Phenotype versus genotype correlation in oligodendrogliomas and low-grade diffuse astrocytomas. Acta Neuropathol. Mar 1.2002 103:267–275. [PubMed: 11907807]
118. Shukuya R, Schwert GW. Glutamic acid decarboxylase: II. spectrum of the enzyme. J Biol Chem. 1960; 235:1653–1657. [PubMed: 14446291]

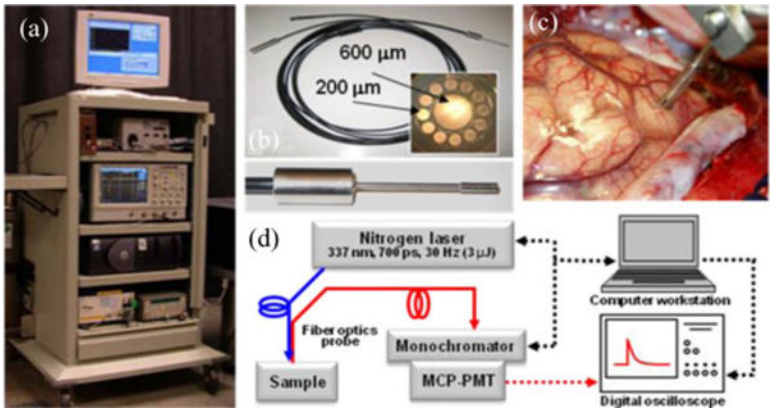

Fig. 1.

(a) Photograph of the TRFS system. (b) Photograph of the fiber optic probe used in clinical setting: inset on the right depicts the fiber front end, and the inset below depicts the tip of the fiber probe. (c) Distal end of the fiber probe positioned on brain cortex; the picture depicts the spacer with two slits allowing for maintaining a fixed distance from the tissue and application of a suction tube to provide a clear field. (d) Schematic of the TRFS system. Adapted from [29].

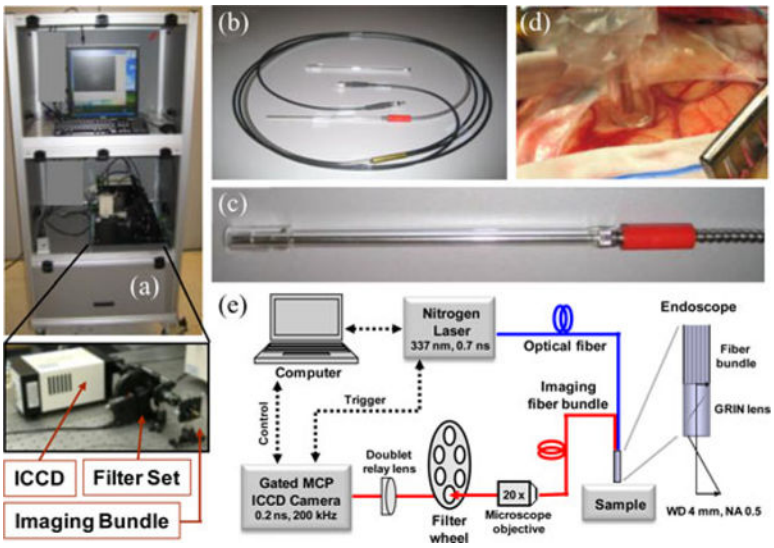

Fig. 2.

(a) Photograph of the FLIM system. (b) Photograph of the imaging bundle probe. (c) Distal end of the probe including an optically transparent spacer. (d) Imaging probe applied to brain cortex. (e) Schematic of the FLIM instrumental setup. Adapted from [34].

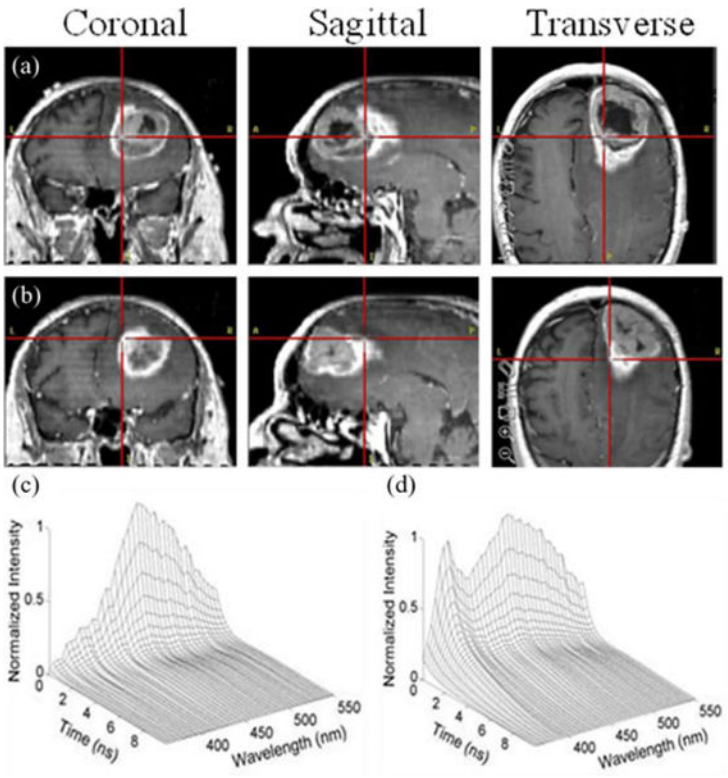

Fig. 3.

Initial identification of areas of interest for TRFS interrogation based on preoperative MRI images. (a) Area within tumor. (b) Area at the tumor margins; typical TRFS point measurement (deconvolved data) from (c) LGG and (d) NWM.

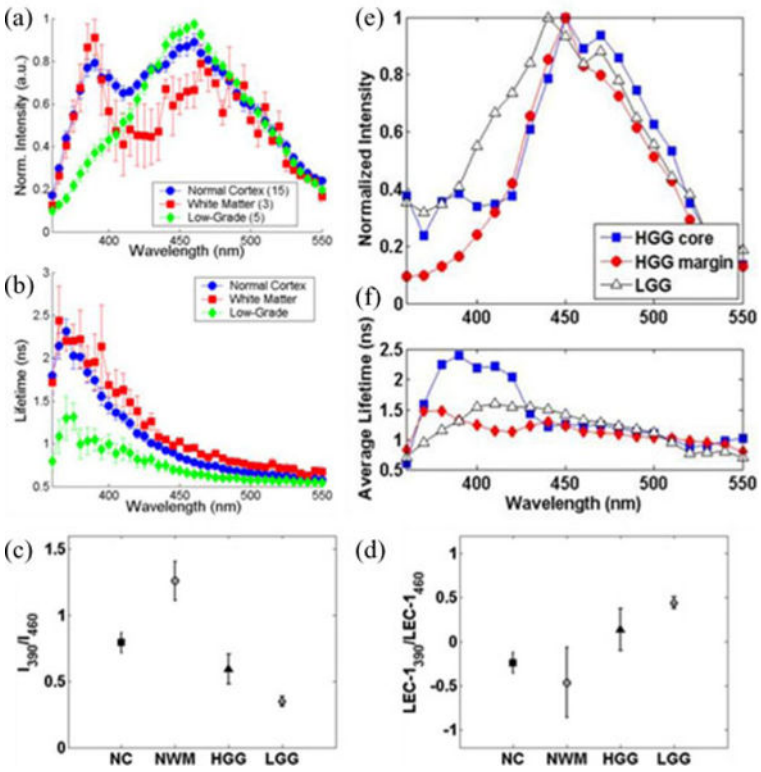

Fig. 4.

Representative fluorescence emission characteristics of distinct brain tissue types (NC, NWM, and LGG). (a) Fluorescence emission spectra. (b) Average fluorescence lifetime. Representative fluorescence parameters (ratio 390 nm versus 460 nm) of (c) absolute fluorescence intensities and (d) Laguerre coefficient (order 1). Adapted from [32]. TRFS features from measurements conducted in two patients: one diagnosed with HGG (measurements conducted in both tumor core and margins) and the other with LLG. (e) Fluorescence emission spectra. (f) Average lifetimes. Note the changes in the fluorescence parameters of HGG (core versus margins of the tumor within the same patient). Also note the differences between the spectroscopic characteristics of HGG and LGG: HHG presents right-shifted peak emission versus LLG and the fluorescence lifetime of the HGG margin is shorter than HHG core, but similar to that of LLG.

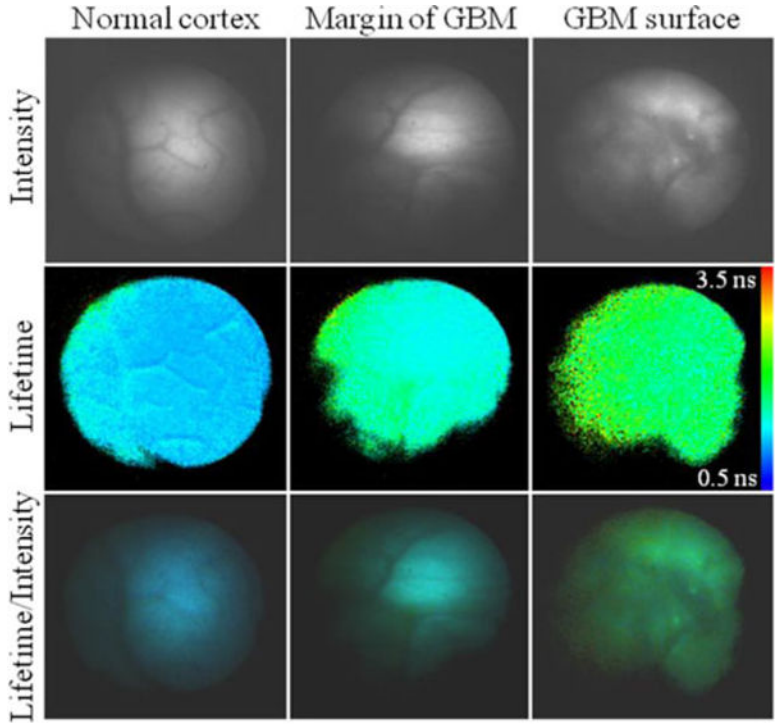

Fig. 5.

(Top) Representative fluorescence intensity, (middle) average lifetime, and (bottom) intensity weighted lifetime images. (Left column) NC. (Middle column) Margin of a GBM. (Right Column) GBM area. For each image, the average lifetime pixel value was retrieved from the binning of four original pixels (2×2 square). Adapted from [34].

TABLE I

Overview of Glioma Resection Standard Care Procedures and New Techniques in Clinical Studies

Standard care	Advantages		Limitations		Resolution and interrogation region size	
Stereotactic Image Guided Surgery with Preoperative Magnetic Resonance Imaging (MRI) Scans [10,11]	–	Allows preoperative, high contrast imaging of the tumor including MRI, Magnetic Resonance Spectroscopy (MRS), Computed Tomography (CT), Positron Emission Tomography (PET)	–	Loss of registration accuracy due to brain shift during surgery	–	MRI image resolution: ~1 mm^3 (3 Tesla unit)
			–	Partially dependent on accuracy of electromagnetic/ optical stereotactic guide	–	MRI field of view (FOV): 20 cm
			–	Provides no pathological information	–	Stereotactic device precision: 2–5 mm
	–	Provides anatomic information				
	–	Shows preoperative blood-brain-barrier leaks				
Intraoperative Ultrasound [12–17]	–	Shows real time tracking of intraoperative brain shift during operation	–	Lower resolution and unable to accurately distinguish between tumor/ hemorrhage/ edema	–	Transducer frequency range: 5–15 MHz
	–	Can correct for brain shift in MRI and CT images	–	Steep learning curve requires extensive experience	–	Resolution: 0.15–0.35 mm (axial), 0.4–1.2 mm (lateral)
	–	Inexpensive and readily available	–	Requires an interruption of all surgical procedures while the scan is performed	–	Penetration: 3–10 cm
					–	FOV: 20×20 mm
Intraoperative MRI (iMRI) [18–21]	–	Provides high resolution structural information	–	High costs for the systems and the associated operating room modifications	–	Resolution: ~1.5 mm (~3–5 mm slice thickness)
	–	Can identify areas of tumor located beneath the surface	–	Does not always identify the low-grade tumor and does not enhance with gadolinium	–	Acquisition time: 3–8 minutes
	–	Corrects for any brain shift during surgery	–	Requires an interruption of all surgical procedures	–	FOV:~20 cm (256×256 matrix)
	–	High field units can be used for MRS			–	Spatial resolution is proportional to magnetic field strength

Standard care	Advantages		Limitations		Resolution and interrogation region size	
		& functional MRI		while the scan is performed		
Surgical Biopsy	–	Provides accurate information about tumor pathology and assists in diagnosis and subsequently prognosis	–	Irreversible and can cause neurological deficits	–	Typically 1–2 mm in diameter
			–	Unusable in areas of the functional cortex		
			–	Requires 15–20 minutes for tissue processing		
New techniques in clinical studies	**Advantages**		**Limitations**		**Resolution and interrogation region size**	
Exogenous Contrast Agents (FGR) [22, 23]	–	Quick learning curve for surgeons	–	Contrast agent injection may cause allergies or interactions with other drugs	–	Resolution not well characterized due to variability in agent localization and instruments used
	–	Standard neurosurgical microscopes	–	Can cause skin photosensitivity for several weeks after surgery		
	–	modified for fluorescence detection are commercially available	–	Superficial layer of blood can cause significant attenuation of the signal		
	–	May be possible to use contrast agent as an adjuvant photodynamic therapy (PDT) photosensitizer				
Biochemical Imaging Agents (FGR) [24]	–	Tumor tissue discrimination can be easily visualized by the surgeon's eye	–	Ineffective for resecting low-grade gliomas	–	Resolution not well characterized due to variability in agent localization and instruments used
	–	Minimal modifications required to implement in a surgical suite	–	Nonspecific, localizes to atypical tissue (tumorous, necrotic, or demyelinating)		
			–	No strict relationship between degree of proliferation or malignancy and fluorescence		
Diffuse Reflectance & Fluorescence Spectroscopy [25–28]	–	Signal can be correlated to tissue pathology and tumor grade	–	Varying degrees of superficial blood may cause misclassification of tissue	–	Interrogation region: 600×670 μm
	–	Inexpensive and easily incorporated into the operative field	–	Data is collected from a single point source (no structural information)	–	Acquisition time: ~30 sec
					–	Penetration depth: ~500 μm

Standard care	Advantages	Limitations	Resolution and interrogation region size
Fluorescence Lifetime Spectroscopy/Imaging [29–35]	– Signal can be correlated to tissue pathology and tumor grade – Lifetime component is more robust against losses in signal due to blood – Potential for being interfaced with navigational and other surgical and diagnostic tools	– Data is collected from a single point source (no structural information) – Limited penetration depth can make tumors lying below healthy tissue difficult to detect	– Point spectroscopy: ~30 sec for acquisition of fluorescence decays at over 30 wavelengths – Interrogated tissue volume: ~1 mm^3 – Penetration depth: 250–400 μm – FLIM: 2 minute acquisition, 4 mm FOV, ~35 μm spatial resolution – Emerging new techniques: 0.2 μs acquisition time per data point [36, 37]